Steel and Composite Structures, *Vol. 31, No. 4 (2019) 341-359*
DOI: https://doi.org/10.12989/scs.2019.31.4.341

Detection of flaw in steel anchor-concrete composite using high-frequency wave characteristics

Rajanikant Rao [1] and Saptarshi Sasmal [*1,2]

[1] *Academy of Scientific and Innovative Research (AcSIR), India*
[2] *Special and Multifunctional Structures Laboratory, CSIR-Structural Engineering Research Centre, Taramani, Chennai-600113, India*

(*Received November 21, 2018, Revised March 28, 2019, Accepted April 1, 2019*)

Abstract. Non-monolithic concrete structural connections are commonly used both in new constructions and retrofitted structures where anchors are used for connections. Often, flaws are present in anchor system due to poor workmanship and deterioration; and methods available to check the quality of the composite system afterward are very limited. In case of presence of flaw, load transfer mechanism inside the anchor system is severely disturbed, and the load carrying capacity drops drastically. This raises the question of safety of the entire structural system. The present study proposes a wave propagation technique to assess the integrity of the anchor system. A chemical anchor (embedded in concrete) composite system comprising of three materials viz., steel (anchor), polymer (adhesive) and concrete (base) is considered for carrying out the wave propagation studies. Piezoelectric transducers (PZTs) affixed to the anchor head is used for actuation and the PZTs affixed to the surrounding concrete surface of the concrete-anchor system are used for sensing the propagated wave through the anchor interface to concrete. Experimentally validated finite element model is used to investigate three types of composite chemical anchor systems. Studies on the influence of geometry, material properties of the medium and their distribution, and the flaw types on the wave signals are carried out. Temporal energy of through time domain differentiation is found as a promising technique for identifying the flaws in the multi-layered composite system. The present study shows a unique procedure for monitoring of inaccessible but crucial locations of structures by using wave signals without baseline information.

Keywords: steel-polymer-concrete composite; chemical anchor; damage detection; ultrasonic wave propagation; Piezoelectric transducers (PZTs); temporal energy; numerical simulations

1. Introduction

Concrete structures along with steel rods/rebars are being used as anchor system in many engineering fields, including building, tunnelling, mining, dam and bridges. It basically provides a connection between different structural members. It also aims to increase the strength and stability of structures by achieving a robust load transfer mechanism. Many structures possess connections to cater to the design requirement to accommodate the need for assembling structural components of different composite system such as concrete and steel, or concrete and concrete. Further, the recent impetus for fast-track construction has pushed the need for developing the innovative and efficient structural connections (Papastergiou and Lebet 2014, Thirumalaiselvi *et al*. 2016, Sasmal *et al*. 2018). It is found that the connections are one of the most important and complicated regions of the structures. The sound health of the connections would ensure the overall stability and safety of the entire structures (Paknahad *et al*. 2018). Therefore, it is highly important to ensure the structural integrity, safety, and serviceability of such systems. Adhesive or bonded anchors are the most used post-installed anchors in structural connections in which an adhesive layer is used between the interface of concrete and anchor. Technology for using adhesive anchor grouted with an appropriate inorganic agent(s) has been well developed and widely adopted in mining and tunnels. But, with the development of advanced and higher strength organic agents (chemical agents) such as epoxy, polyester and vinyl ester, the use of chemically bonded anchors has drastically been increased in structural engineering applications. Though chemical anchor systems are desired to have very high durability, they are subjected to continuous degradation due to bond failure, poor impact resistance, excessive loads and atmospheric condition such as moisture and temperature variations (Epackachi *et al*. 2015). The other major issue with chemical anchor is the workmanship, due to which many unattended cases lead to failure. The behaviour of the anchor system under both static and dynamic loading condition depends on the interface between the concrete and steel tendon (Puigvert *et al*. 2014, Gou *et al*. 2018). When the interface is severely damaged, such as a micro-crack is formed, debonding can take place or large slip may occur which decreases the load transferring capacity through the interface to another material. It is significant to note that, in most of the cases, the primary load transfer mechanism of connections, i.e., the embedded anchors cannot be accessed or inspected. Thus, the unattended and unmonitored performance of anchor systems put the safety of the entire

*Corresponding author, Ph.D., Professor,
E-mail: sasmalsap@gmail.com; saptarshi@serc.res.in

Copyright © 2019 Techno-Press, Ltd.
http://www.techno-press.org/?journal=scs&subpage=6 ISSN: 1229-9367 (Print), 1598-6233 (Online)

structure in question, and it emphasizes the need for an efficient and continuous monitoring strategy.

Many researchers studied the load transfer mechanism of perfectly bonded anchorage systems by applying different analysing methods (Cook 1993, Yilmaz *et al*. 2013). Since, visual inspection of anchors is not possible and conventional methods such as pull-out tests are destructive, expensive and time-consuming, various non-destructive evaluation/monitoring techniques have been developed. There are two most important groups of diagnostic techniques, namely, free and ambient vibration (global, low frequency) method, and wave propagation method (local, high frequency) which allow the traveling of the wave for a longer distance with little loss in energy (Rong *et al*. 2017, Fourn *et al*. 2018). Non-destructive testing is used for quality control as well as health assessment of infrastructure to provide the information about the internal condition of the concrete system (Lee *et al*. 2017). But, the problem with NDT method is that it can provide mainly offline safety and the problem of accessibility restricts its application (Adams 2007).

In recent years, techniques based on ultrasonic guided waves have gained popularity and played a vital role in the structural health monitoring (SHM) of civil infrastructures. Structural health monitoring is a technique for executing the integrated sensing/actuating system to evaluate the state of health of structures and identify the damages based on data acquisition and processing (Mohseni and Ng 2018). SHM has the capability of testing over long periods of time with higher sensitivity and the ability to test the multi-layered structures for establishing a real-time non-destructive monitoring system (Zheng and Lei 2014). It can facilitate the online monitoring and assessment of structures economically in lesser time (Adams 2007). Earlier, researchers (Neilson *et al*. 2007, Song *et al*. 2017) have used the vibrational signature for damage detection, by using low frequency. Due to the lack of sensitivity of low frequencies for localised damage cases, these techniques are, most of the times, unable to detect the damage properly.

Recently, using the light and very sensitive smart materials like piezoelectric transduces (actuator/sensor), studies on wave propagation techniques have gained momentum (Akbas 2015, Song *et al*. 2017). Raghavan (2007) presented an exhaustive review of techniques for structural health monitoring using guided waves. Song *et al*. (2006) and Wang *et al*. (2013) developed intelligent (smart) materials transducers with guided waves for the structural health monitoring and rehabilitation of concrete structures. Haynes *et al*. (2014) carried out a parametric study for the monitoring of bearing failure in composite bolted connections using ultrasonic guided waves. Zheng and Lei (2014) proposed an analytical/numerical method to investigate the effect of concrete on propagation characteristic of guided waves in steel bar embedded in concrete. It was brought out that the velocity and attenuation of propagating wave are greatly affected by the presence of aggregate (fine and coarse) in concrete; while Hsiao *et al*. (2008) investigated the impact response of concrete blocks for the feasibility of using the impact-echo method for detection of flaws in a concrete block. Kocaturk and Akbas (2013) investigated the influences of the material length scale parameter(s) on the wave propagation in a micro beam based on the modified couple stress theory. Similarly, Akbas (2014) found that the wave propagation techniques can be easily used for crack detection within structures by obtaining additional waves. Akbas (2016) conducted his further studies on the wave propagation in an edge cracked cantilever beam composed of functionally graded material under the effect of an impact load. It was observed that the material distribution plays an important role in the wave propagation of the functionally graded beam with cracks.

On the other hand, due to a strong piezoelectric effect, wide frequency band, quick response, low cost and the capacity of both actuating and sensing, monitoring of structures using piezoelectric transducers (PZTs) emerged as one of the modern methods of structural health monitoring (Song *et al*. 2008b and Yan *et al*. 2009). For the damage detection, localization and size determination, pitch-catch (Ihn *et al*. 2008) and pulse-echo (Giurgiutiu 2011) methods were experimentally and numerically demonstrated. Song *et al*. (2007) used embedded piezoceramic transducers in the concrete structure at pre-determined spatial location to predict the failure of concrete structures. An experimental study was performed by Divsholi *et al*. (2008) using PZT sensors for the detection of damage location and severity level; and Yang *et al*. (2008) used the PZT electro-mechanical admittance signature as the damage indicator for detection of structural damages in a 2-storey RC frame. Further, PZT sensors bonded on steel reinforcing bars that were embedded in concrete specimens were also applied to perform non-destructive testing and evaluation of the bond development between bar and concrete (Tawie and Lee 2010). Liu *et al*. (2016) presented a detection method for the damage in plate-like structure with a compact rectangular phased piezoelectric transducer array of 16 piezoelectric elements. These compact arrays are capable of detecting and locating a single defect in plate, as well as identifying multi-defects. While Hall and Michaels (2015) introduced a multipath guided wave imaging technique to detect damage in aluminium plates. Similarly, an integration approach based on both electromechanical admittance and guided wave propagation technique was used to evaluate the damage on the steel bar by Providakis *et al*. (2014) and Karayannis *et al*. (2016). It was observed that the damage can be the result of excessive elongation of the steel bar due to steel yielding or due to local steel corrosion. Chalioris *et al*. (2015) used embedded and externally bonded piezoelectric transducers to evaluate a shear-critical reinforced concrete beam. The experimental study carried out by Zhang *et al*. (2018) showed that the amplitude of the signal attenuates with the presence of damage in the joints, and the degree of attenuation increases with the development of the damage. The active interface debonding detection for concrete-filled steel tubes (CFSTs) using PZT patches was experimentally studied by Xu *et al*. (2017). Numerical results demonstrated that interface debonding leads to changes in guided wave propagation RodjdlTsms wkpath, traveling time and the sensor response. Ultrasonic guided waves actuated and received by surface-bonded piezoelectric wafers were simulated and used to quantitatively evaluate the debonding between concrete beams and carbon fibre reinforced polymer (CFRP) overlay by Li *et al*. (2017) at the excitation frequency 50 KHz.

Recently, attention has been paid towards time reversal method (TRM) in the field of guided wave-based techniques to improve the detectability of local defects in different composite structures (Park *et al*. 2007, Wang *et al*. 2015). Many researches performed theoretical as well as experimental investigations on different structures. Gangadharan *et al*. (2009) investigated an active sensing using Lamb waves health monitoring of a metallic structure. Mustapha *et al*. (2014) used time reversal method in rebar-reinforced concrete beam for damage detection. Agrahari and Kapuria (2016) proposed the time-reversed Lamb wave-based baseline-free damage detection technique for notch-type damage in isotropic plates.

The previous studies showed a huge potential of the application of guided waves in health monitoring of chemical anchors, especially in assessing of effects of insufficient rebar, missing grout (Cui and Zou 2012, Yu *et al*. 2013), identification of free length of an anchor (Wang *et al*. 2009, Zou *et al*. 2010) and identification of basic geometric parameters. However, the number of studies for detection of debonding between steel and concrete using wave propagation techniques are limited. Gu *et al*. (2016) proposed a monitoring technique for reinforced concrete using an active diagnosis method to assess the debonded state between the steel bars and concrete. Amjad *et al*. (2015) conducted an experimental analysis for detection and quantification of corrosion level in reinforced steel bar, while Rajeshwara *et al*. (2017) attempted to correlate the combined effect of corrosion and debonding and established a method to quantify the level of damage using wave propagation techniques in a three-dimensional reinforced concrete beam. Analytical and computational studies were presented by Seifried *et al*. (2002) to provide a quantitative understanding on the propagation of guided waves in multi-layered adhesive bonded components, where the effect of the adhesive bond layer including low stiffness and viscoelastic behaviour were the key focus of the study. An experimental study was carried out by Contrafatto and Cosenza (2014) to investigate the applicability of numerical models for the prediction of bearing capacity of chemical anchors. An investigation was performed to detect the debonding in reinforced concrete structures by Wu and Chang (2006). In this study, parametric analysis, intensity analysis and the moment tensor analysis of acoustic emission data were used to distinguish the different sources of damage. Recently, Zima and Rucka (2015) conducted a novel experimental study on wave propagation in laboratory models of ground anchors with different bonding length and different frequencies of excitation. Experimental results showed that as the bonding length increases, more wave energy can be transferred into concrete and the amplitude quickly attenuates. Further, they reported the investigations of efficacy of ultrasonic waves for evaluation of damage in steel bars partially embedded in mortar. Shen *et al*. (2018) carried out a numerical simulation on wave propagation in reinforced concrete structures with debond damage.

Based on above studies and observations, it is found that most of the studies are on homogeneous isotropic medium. Further, on anchor or rebar/bond like problem also, instrumentation was primarily done on rebars only. In case of anchor, it will be a completely different scenario. Here, the anchor head and surrounding concrete is accessible, not the other end of the anchor, which makes the problem complex and poses a great challenge to develop an appropriate method for damage detection of such system using ultrasonic wave propagation. The novelty of the present study lies in developing the methodology where three phenomenons are effectively considered: (i) propagation of guided wave through the wave guide (anchor); (ii) transmission of leaky wave to concrete through the chemical interface; and (iii) the received signal from bulk wave propagated through the concrete. The received signal is analysed to develop an efficient method for damage detection in chemical anchors embedded in concrete. Further, developing the baseline free damage detection method for such composite system is another challenge which is successfully addressed in this study as well. In the present study, chemical anchor systems (embedded in concrete) are considered for carrying out the wave propagation studies in the composite (steel anchor-polymer adhesive-concrete) medium. Three cases are considered with different interface and the same are experimentally investigated. Further, numerical models are developed using finite element method and results obtained from the numerical studies are validated with experimental results. The validated numerical models enable to carry out a detailed wave propagation study on a composite system made of steel rod-epoxy interface-concrete base and evaluate the influence of the key parameters and critical wave signatures. Further, the actuator-receptor wave information obtained from various cases obtained from numerical studies is suitably analysed to assess the presence of any flaw or defect in the anchor system. In the nutshell, the present study is focussed on developing the experimentally validated numerical models and baseline free damage detection technique for identification of flaws (which are inside the embedded matrix and inaccessible) in chemical anchor system using ultrasonic wave propagation.

2. Theoretical background of wave propagation in cylindrical guided waves

The investigations conducted in this paper are focused on the guided wave propagation in a cylindrical steel bar partially embedded into the concrete, with and without epoxy layer between the interfaces. When an elastic wave is excited and starts to propagate along the free bar, various modes of waveguides are generated. However, in steel rod, the nature of propagation of waves is dispersive having three types of propagating modes, such as longitudinal, torsional and flexural modes. Guided waves can propagate only in structures where the energies are concentrated near the boundaries (Song *et al*. 2017). It can occur when reflection and refraction take place through the boundary region over a long distance and can be excited using a short duration of tone-burst. The analytical formulation for three-dimensional wave motion in a solid cylinder was first developed by Pochhammer and Chree, and the solution (describes longitudinal, torsional and flexural wave propagation) is known as Pochhammer-Chree solution. The Pochhammer-Chree frequency equation for the longitudinal modes can be written as (Rose 2004)

$$\frac{2\alpha}{r}(\beta^2+k^2)J_1(\alpha a)(\beta a)-(\beta^2-k^2)^2 J_0(\alpha a)J_1(\beta a)$$
$$-4k^2\alpha\beta J_1(\alpha a)J_0(\beta a)=0 \tag{1}$$

Were 'a' is the radius of bar and J_0 and J_1 denote Bessel's functions of the first kind. The parameters α and β depend on the wavenumber k and the angular frequency ω

$$\alpha^2=\frac{\omega^2}{{C_L}^2}-k^2, \qquad \beta^2=\frac{\omega^2}{{C_s}^2}-k^2 \tag{2}$$

Where, C_L and C_T are the velocity of longitudinal and transverse waves respectively for free rod which can be define as

$$C_L=\left(\frac{E(1-\upsilon)}{\rho(1+\upsilon)(1-2\upsilon)}\right)^{1/2} \tag{3}$$

$$C_T=\left(\frac{E}{2\rho(1+\upsilon)}\right)^{1/2} \tag{4}$$

Where, E, ρ and υ are the Young's modulus, density and poison's ratio of materials respectively. By solving Eq. (1), we can obtain the frequency dispersion characteristics. The phase velocity (C_P) and group velocity (C_g) can be calculated at a given frequency using Eq. (5). The graphical representation of this solution is known as dispersion curve which is relating the phase or group velocity to the wave frequency ω.

$$C_g=\frac{d\omega}{dk}, \qquad k=\frac{\omega}{C_p} \tag{5}$$

The group velocity dispersion curves for a steel bar with diameter of 12 mm are typically presented in Fig. 1. The bar diameter is chosen in such a way that the same is used in the experimental and numerical investigations of the present study. It is important to note from the dispersion curve that, upto 250 kHz only one longitudinal mode can propagate and afterward torsional and flexural waves are generated. This information helps in choosing the frequency range for the study so that the uncoupled modes can transfer and the desired leakage to the concrete medium can be maximised.

The characterization of wave dispersion is well established and reported by many researchers (Amjad *et al.* 2015, Rajeshwara *et al.* 2017). But, when waves are propagating in a steel rod embedded into different materials, the guided waves propagate not only along the steel rod but also spread outward, which leads to the diffusion of the wave energy from steel to different medium as shown in Fig. 2. These interactions of energies between interface of two different mediums depend on mechanical

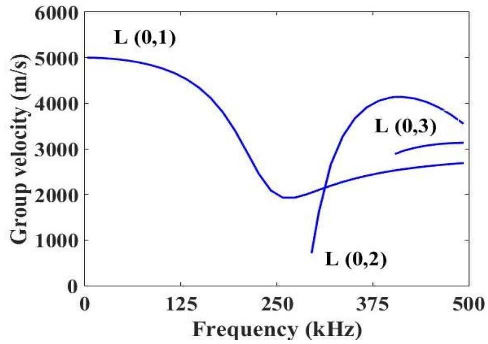

Fig, 1 Group velocity dispersion Curve for 12 mm dia. steel rod (E = 200 GPa, v = 0.3, ρ = 7850 kg/m^3

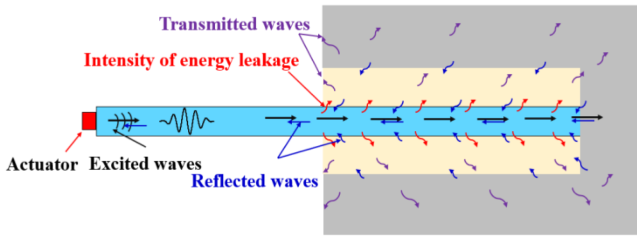

Fig. 2 Wave propagation in layered media

properties, geometric arrangements, nature of interfacial interaction and loading condition. At the interface, transmission and reflection of the guided waves take place based on the material properties of both medium and angle of wave attack. More detailed discussion on the same can be found in Rose (2004).

The intensity of transmission and reflection depends on acoustic impedance (resistance capacity) of media due to different material parameters such as density and modulus of elasticity (Rucka and Zima 2015). If the difference between the impedances of the mediums is large, the amount of reflection of waves will be high. The amplitude, as well as energies of these waves, get attenuated because of leakage of energy between the interface of materials. Intensity of wave energy depends not only upon the material properties but also on the strength of bonding, bonding length and quality of the connection between the interfaces. If the connection between the interfaces is perfect, then maximum amount of wave energy gets transferred from one medium into the other. Therefore, the main problems in this type of cases are mainly bonding strength and bonding length. Bond strength deteriorates due to corrosion of steel rod which leads to the damage to the structures and which further causes its failure or collapse.

3. Numerical simulation using finite element analysis

3.1 FEA model

In the present study, implicit analysis module of ABAQUS was used for numerical simulation. The implicit model uses an automatic increment strategy based on success rate of a full Newton iterative solution method

$$\Delta \boldsymbol{u}^{(i+1)} = \Delta \boldsymbol{u}^{(i)} + \boldsymbol{K}_t^{\,-1}.(\boldsymbol{F}^{(i)} - \boldsymbol{I}^{(i)}) \tag{6}$$

Where, K_t is the tangent stiffness matrix, $\boldsymbol{F}$ is the applied load vector, '$\boldsymbol{I}$' is the internal force vector, and $\Delta \boldsymbol{u}$ is the increment of displacement. For an implicit dynamic procedure, the algorithm is defined by Prior (1994)

$$\boldsymbol{M}\ddot{\boldsymbol{u}}^{(i+1)} + (1+\alpha)\boldsymbol{K}\boldsymbol{u}^{(i+1)} - \alpha \boldsymbol{K}\boldsymbol{u}^{i} = \boldsymbol{F}^{(i+1)} \tag{7}$$

Where **M** is the mass matrix, **K** is the stiffness matrix, **F** is the applied load vector and **u** is the displacement vector

$$\boldsymbol{u}^{(i+1)} = \boldsymbol{u}^{(i)} + \Delta t \dot{\boldsymbol{u}}^{(i)} + \Delta t^2 \left(\left(\frac{1}{2} - \beta \right) \ddot{\boldsymbol{u}}^{(i)} + \beta \, \ddot{\boldsymbol{u}}^{(i+1)} \right) \tag{8}$$

and

$$\dot{\boldsymbol{u}}^{(i+1)} = \dot{\boldsymbol{u}}^{(i)} + \Delta t \left((1-\gamma)\ddot{\boldsymbol{u}}^{(i)} + \gamma \ddot{\boldsymbol{u}}^{(i+1)} \right) \tag{9}$$

With

$$\beta = \frac{1}{4}(1-\alpha^2), \quad \gamma = \frac{1}{2} - \alpha, \quad \frac{1}{3} \leq \alpha \leq 0 \tag{10}$$

α = -0.05 is chosen (default values in ABAQUS) as a small damping term to quickly remove the high frequency noise without having a significant effect on the lower frequency response.

3.2 Model implementation

The simulation of the wave propagation with piezo-electric (PZT) transducers was carried out using ABAQUS(Implicit standard module). Steel, concrete and epoxy were modelled using the 3D stress eight noded linear brick element (C3D8R) with reduced integration and the piezoelectric actuator and sensor were modelled with the eight noded linear piezoelectric brick element (C3D8E). The interfaces between the piezoelectric elements and the steel rod and concrete were electrically grounded. Since the piezoelectric patches are considered as electrodes on the surfaces, these surfaces are equipotential. This was achieved by coupling the electric potential degrees of freedom of the nodes on the outer piezoelectric surfaces, using the interaction constraint equation feature of ABAQUS. The actuating/sensing element can be directly simulated by applying electric voltage. The additional degree of freedom in this coupled field element is the electrical voltage. Input voltage is applied to the top nodes of the PZT actuator, and zero voltage is assigned to all the bottom nodes of the PZT actuators and sensors to simulate the grounding operation.

A concrete block with a dimension of 300 mm × 300 mm × 150 mm, anchor steel rod with 12 mm diameter and 150 mm long with 16 mm diameter of steel rod head and 5 mm thick head is considered. The same was numerically instrumented using three PZT transducers (actuator/sensors) of dimension 10 mm × 10 mm × 0.25 mm. Steel rod was embedded exactly in the middle of concrete block up to 100 mm depth, and 50 mm rod length was used as a free length. For analysis purpose, three different models were simulated. The first model was created without an epoxy layer between the interfaces of concrete-steel and called as a fully-bonded case (Fig. 3(a)). The second model was with an epoxy between the interface of steel-concrete and called as a full epoxy case (Fig. 3(b)); while the third model presented epoxy but only till half portion of steel embedded depth from the top surface of concrete and called as a half epoxy case (Fig. 3(c)). In half epoxy case, lower interface behaves as a free space which is considered as the damaged model. In full epoxy and half epoxy model, 1 mm thick adhesive layer was used between concrete and steel rod interface. The thickness of epoxy glue between PZT and steel or concrete was 50 micro-meters.

A PZT patch was attached at the top of steel rod head, which was used as an actuator while two PZT patches (S1 and S2) are attached to the concrete surface for sensing purpose. The distances of the first sensor (S1) and the second sensor (S2) from the center of the anchor were 45 mm and 90 mm, respectively. The geometry of the typical specimen is presented in Fig. 4. For reducing the computational time, due to the symmetry of the problem, only one-fourth volume of materials is considered for simulation, as shown in Fig. 5. To avoid the very common problem of insufficient sampling of data along the space

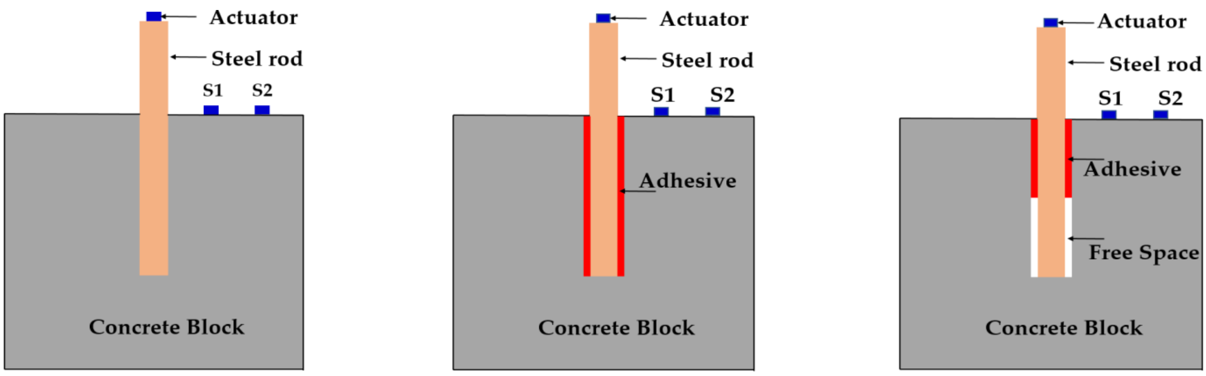

(a) Case1 (Full Bonded) (b) Case 2 (Full Epoxy) (c) Case 3 (Half Epoxy)

Fig. 3 Full bonded, full epoxy, half epoxy (damage model) front view 2-D model

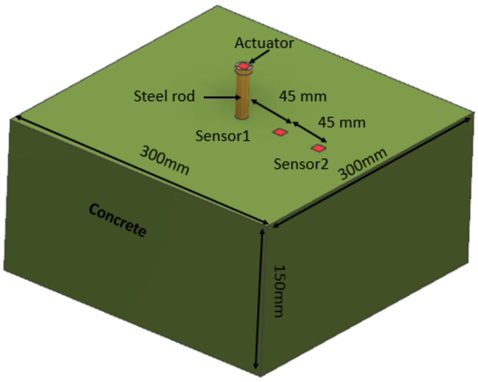

Fig. 4 Full anchor model

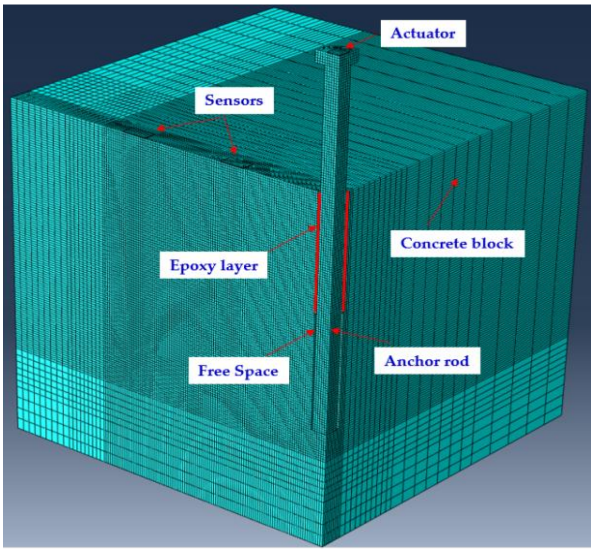

Fig. 5 One fourth mesh model with half epoxy

axis during finite element discretization and for faster convergence of dynamic simulations, meshes of the structures are to be fine enough (at least 20 elements per wavelength) along the direction of wave propagation (Song *et al*. 2008a). From analytical studies of wave propagation, it is observed that the lowest phase velocity occurs due to transverse wave speed which can be used to compute the shortest wavelength ($\lambda_m = \frac{C_T}{f}$) to set the maximum permissible grid spacing. Further, the time increment for transient analysis must be much lesser than the time required for a wave with maximum velocity (C_L) to travel the distance between adjacent nodes (l_e) and is given by $\Delta t \leq \frac{l_e}{C_L}$. Thus, if l_e satisfies the element mesh size criteria $l_e \leq \frac{\lambda}{20}$, the above time increment also satisfies the requirement of at least 20 steps during one wave cycle i.e., $\Delta t \leq \frac{1}{20\,f}$ (Agrahari and Kapuria 2016, Han *et al*. 2009). Hence, the element mesh size and time increment for all frequency up-to 100 kHz along the wave propagation path are 1 mm and 100 ns, respectively. The numbers of elements and nodes for full bonded model are 484868 and 510389 for full epoxy model 485046 and 510950 while for half epoxy model are 484546 and 509850. On the top of the model, free boundary is considered, while on the bottom of model the displacement as well as rotation along *x*, *y* and *z* direction are assigned to be zero (arrested). ''Tie'' constraints are used between the interface of two parts for perfect connection by considering no relative slip between interfaces. A narrow bandwidth Hanning window with modulated sinusoidal five cycle tone burst signal (Eq. (11)) is employs for actuation and is shown as (Fig. 6)

$$V(t) = A * (0.5 * (1 - \cos(2 * pi * f * \frac{t}{n}))) * \sin(2 * pi * f * t) \tag{11}$$

Where A = Amplitude of applied voltage and n is number of cycles. For the present study, concrete, steel and adhesive are considered to behave as elastic homogeneous materials. Properties of materials used in the numerical simulation are listed in Tables 1-2.

Table 1 Material properties of concrete (Song *et al*. 2008a), steel (as specified by Vendor) and Epoxy (Agrahari and Kapuria 2016)

Material	Density (kg/m^3)	Young's modulus (GPa)	Poisson's ratio
Concrete	2400	22.5	0.21
Steel	7850	200	0.3
Epoxy	1700	4.7	0.4

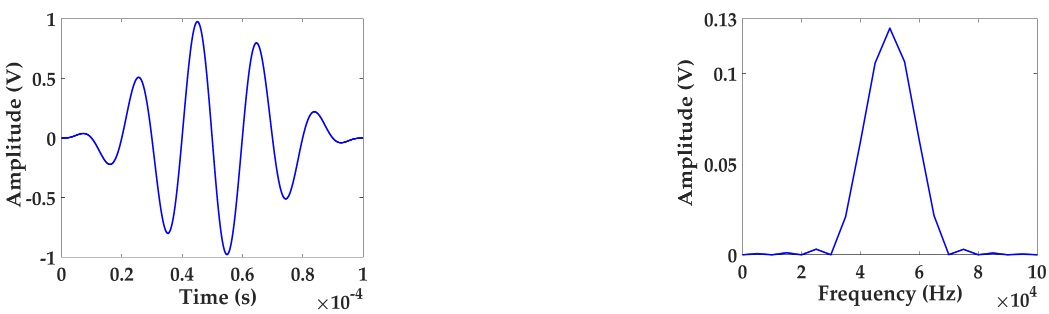

(a) (b)

Fig. 6 (a) Five-cycle Hanning window modulated sinusoidal tone burst excitation with 50 kHz central frequency; (b) The frequency spectrum

Table 2 PZT patch material properties (Agrahari and Kapuria 2016)

Material	E_1 (GPa)	E_2	E_3	G_{12}	G_{13}	G_{23}	υ_{12}	υ_{12}	υ_{12}	P (kg m^{-3})
PZT SP-5H	66.67	66.67	47.62	23.50	23.00	23.00	0.29	0.51	0.51	7500
	d_{31}	d_{32}	d_{33}	d_{15}	d_{24}	$\varepsilon_{11}/\varepsilon_0$	$\varepsilon_{22}/\varepsilon_0$	$\varepsilon_{33}/\varepsilon_0$		
	$\times 10^{-12}$ mV^{-1}									
	-265	-265	550	-	-	3100	3100	3400		

4. Experimental validation

Experimental investigation was carried out to validate the finite element simulation results for first two model i.e., full bonded and full epoxy where actuations was done using the frequency of 50 kHz. Both the models were of same dimensions as that used in the numerical study. Specimens were made of concrete (cement, water, coarse aggregate, and fine aggregate), with water/cement ratio of 0.3 and the fine/coarse aggregates ratio of 0.5. The procedure for preparing the specimens is shown in Fig. 7. The specimens were taken out after 28 days of water curing. After curing, a 14-mm diameter hole was created exactly in the middle using a drill bit to install the steel anchor (Fig. 7). In full epoxy case, a layer of adhesive (Araldite epoxy) was used for perfect connection between steel and concrete interface, while for the full bonded case, steel anchor was inserted during casting itself. The flowchart and experimental setup is schematically shown in Fig. 8. The experimental setup consists of (1) an arbitrary function generator (KEYSIGHT 33500B series waveform generator), (2) a wideband amplifier (TREK INC Model PA05039), (3) a digital Oscilloscope (DSO1002A, 60 MHz, 2Analog Channels), (4) a personal computer, (5) Concrete embedded anchor

(a) Cement

(b) Coarse aggregates

(c) Fine aggregates

(d) Mixing of material

(e) Casting of sample

(f) Finished sample

(g) Anchor system

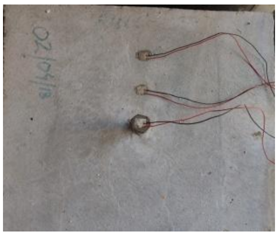

(h) Sample with PZT Patch

Fig. 7 Sample preparation

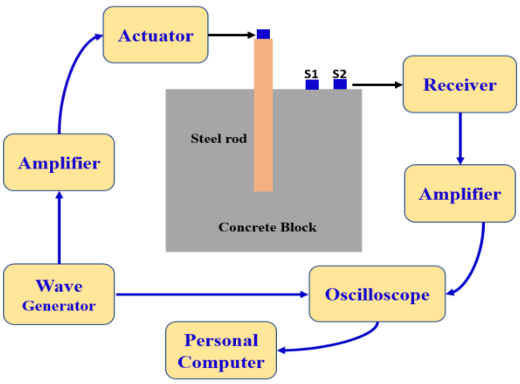

(a)

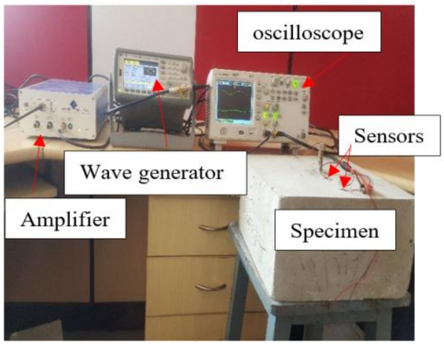

(b)

Fig. 8 (a) Flowchart for experimented setup; and (b) full set-up for the experiment system. Due to high attenuation of wave energies during its propagation in concrete, the actuating signal on actuator should be strong enough to generate a sensible output at the receiver end. An amplifier was used to amplify the signals from the wave function generator as well as the receiver. Peak to peak value of 20 V narrow band five-cycle sinusoidal Hanning window modulations were applied from the function generator to actuate the mounted PZT patch at different frequency level (12.5-100 kHz). Signals from sensors (receivers S1 and S2) were amplified and collected by a digital oscilloscope. Further the collected data are processed in the personal computer. The sample data acquired are averaged in the data acquisition hardware of oscilloscope. A 128-sample data bin was selected for averaging to reduce the noise and to acquire the clear wave pattern. Due to the very high sensitivity of the transducers to vibration, noise reduction is essential.

The experimental results obtained from both sensors (S1 and S2) at 50 kHz frequency are compared with the results obtained from the numerical studies (Figs. 9-10). The numerical results are found to be well corroborated with the experimental results. The quantitative similarities between the signals obtained from experimental and numerical investigations are computed and presented in Table 3. The calculation of similarities between two signals has been discussed (Eq. (12)) in more detail in time reversal method, under section 5.1.2. After validating the numerical models, the same was used for detailed numerical studies for integrity assessment.

Table 3 Quantitative similarity between numerical and experimental results

Model	Sensor1	Sensor2
Full bonded	96.08 %	93.05 %
Full epoxy	98.83 %	97.44 %

5. Results and discussion

Numerical investigations were conducted to simulate the guided wave with an excitation frequency of 12.5, 25, 50, 75 and 100 kHz. The input excitation wave signal was used at a constant voltage of 20 V. The sampling time for 50 kHz and 100 kHz was 200 μs while for 12.5 kHz and 25 kHz, was 600 μs. The output-response signal was obtained from sensors (S1 and S2) which are attached to concrete top surface. Due to high attenuation of waves in concrete, not much energy was available for low-frequency waves to reach the sensors mounted on concrete surface. Thus, sensors S1 and S2 were unable to capture any (or very little)

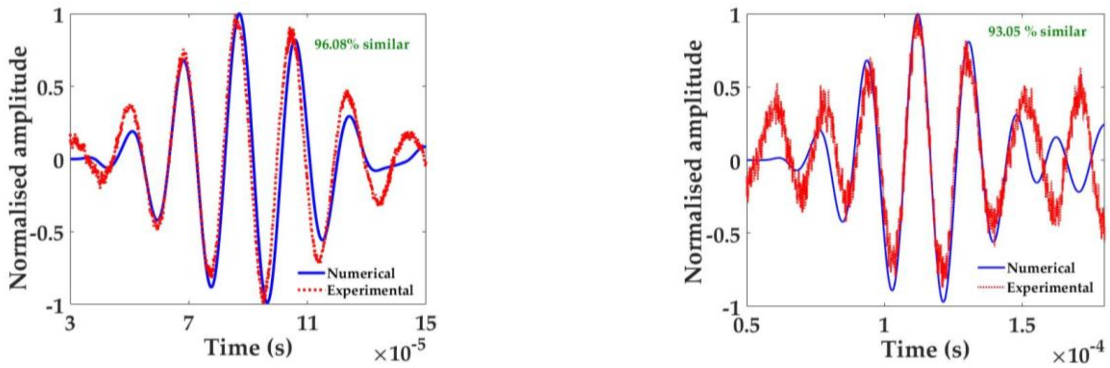

(a) (b)

Fig. 9 Comparison of experimentally obtained (a) sensor1; and (b) sensor2 with numerically obtained results at frequency 50 kHz for full bonded specimen

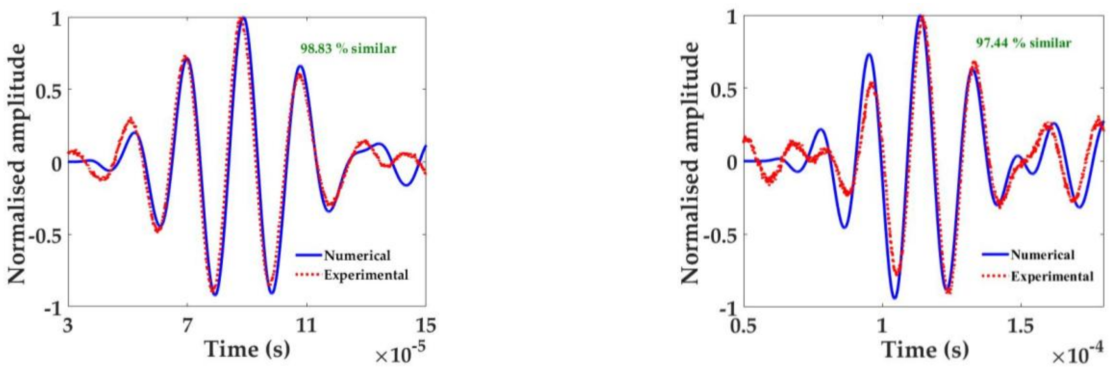

(a) (b)

Fig. 10 Comparison of experimentally obtained (a) sensor1; and (b) sensor2 with numerically obtained results at frequency 50 kHz for full epoxy specimen

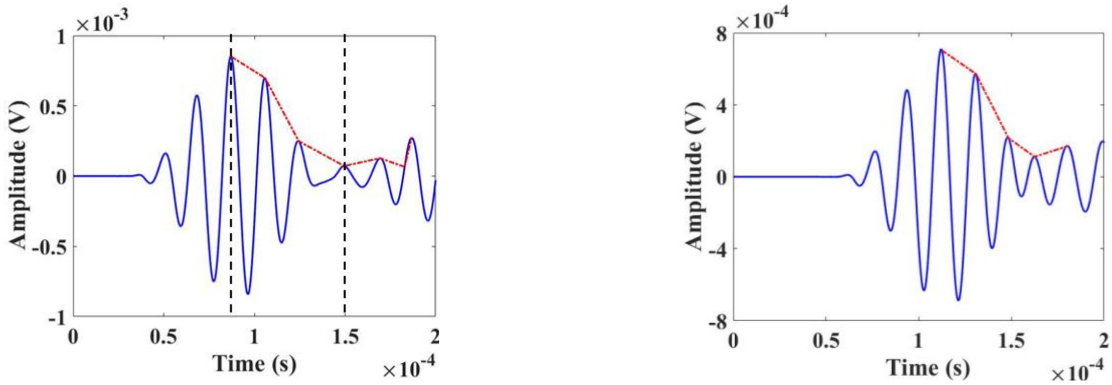

(a) (b)

Fig. 11 Response signal from (a) sensor 1 (S1); and (b) sensor 2 (S2) at frequency 50 kHz for full bonded model

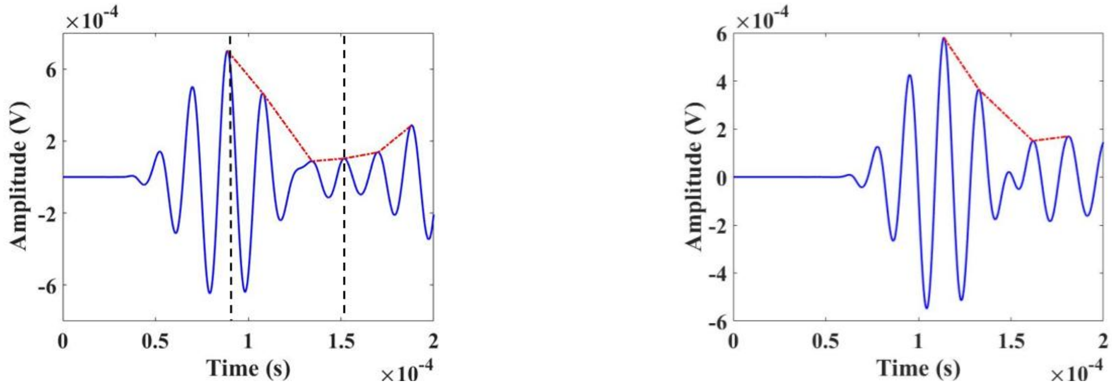

(a) (b)

Fig. 12 Response signal from (a) sensor 1 (S1); and (b) sensor 2 (S2) at frequency 50 kHz for full epoxy model

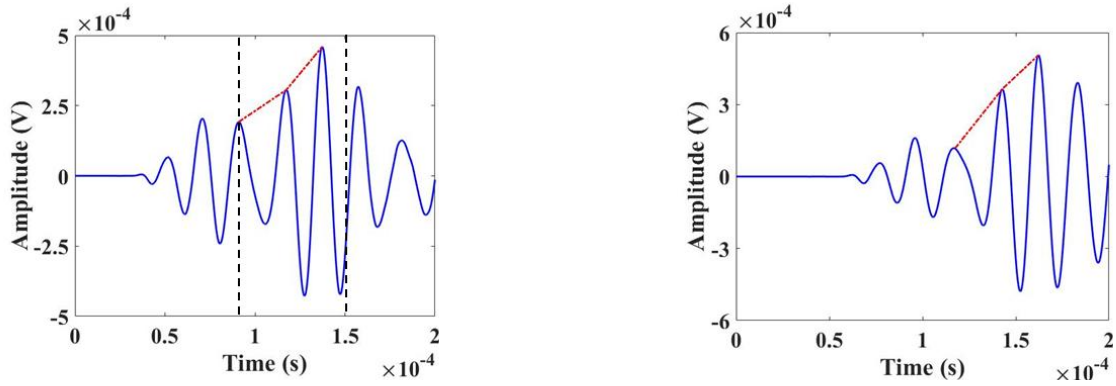

(a) (b)

Fig. 13 Response signal from (a) sensor 1 (S1); and (b) sensor 2 (S2) at frequency 50 kHz for half epoxy or damage model

wave signal from the concrete block when excitation frequency is below 25 kHz. Further, at the very high frequency, the intensity of reflected signal as well as the noise level in the concrete is found to be very high. In that case, it is very difficult to differentiate between response signal and the reflected signal. At a frequency of 25 kHz, sensors S1 and S2 can detect the wave response from concrete block. However, frequencies between 50 kHz and 75 kHz provide better response for detecting damages/flaws inside the concrete matrix. The results obtained from sensors S1 and S2 at a frequency of 50 kHz and 75 kHz at 20V excitation signal are presented in Figs. 11-16. Figs. 11 to 13 are obtained at 50 kHz excitation frequency for different models, while Figs. 14 to 16 is obtained at 75 kHz from sensor S1 and S2. As mentioned earlier, for all the cases (full bonded, full epoxy and half epoxy case) the material properties (concrete and epoxy and steel) are considered as elastic and isotropic. It is clear from the healthy models (full bonded and full epoxy) that the wave response envelops first started to increase and reaches its

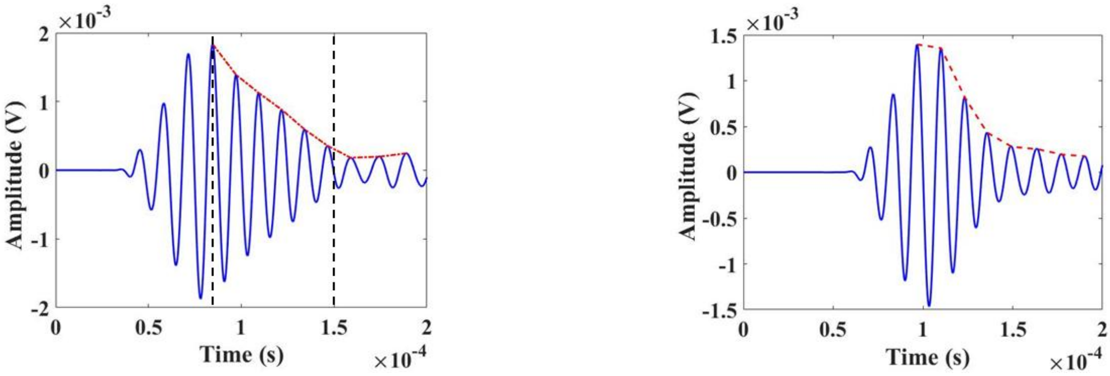

(a) (b)

Fig. 14 Response signal from (a) sensor 1 (S1); and (b) sensor 2 (S2) at frequency 75 kHz for full bonded model

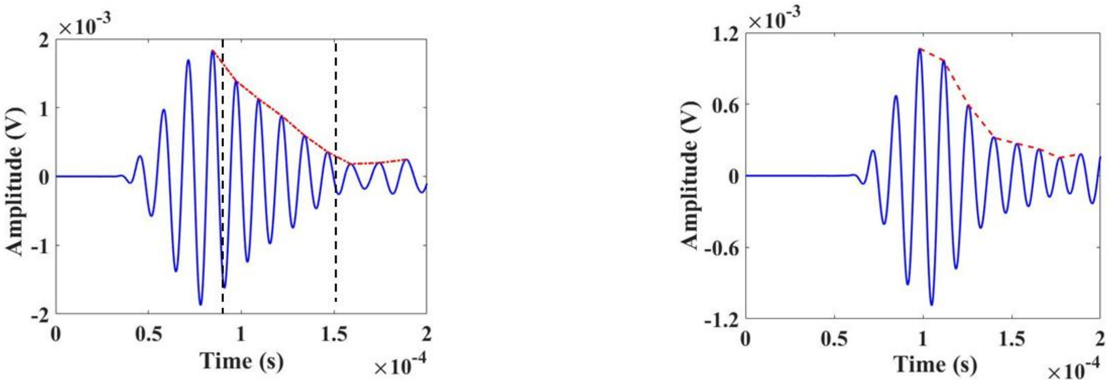

(a) (b)

Fig. 15 Response signal from (a) sensor 1 (S1); and (b) sensor 2 (S2) at frequency 75 kHz for full epoxy model

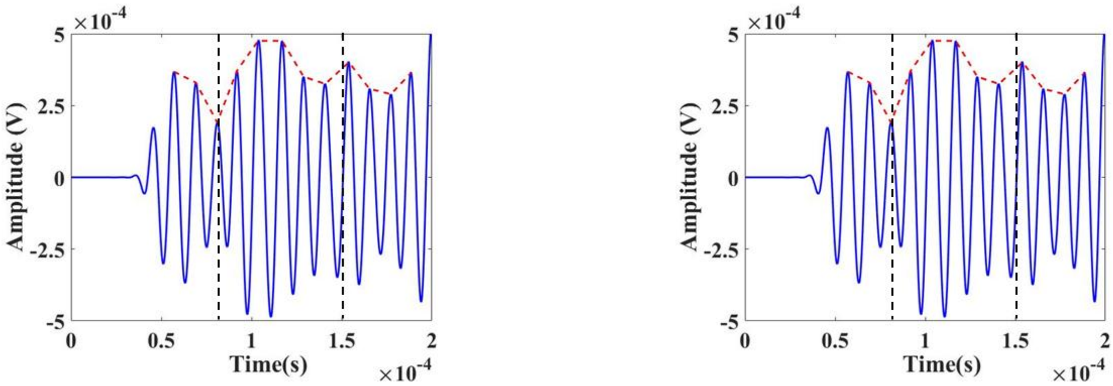

(a) (b)

Fig. 16 Response signal from (a) sensor 1 (S1); and (b) sensor 2 (S2) at frequency 75 kHz for half epoxy or damage model

peak amplitude, and after which it starts to decrease. Whereas if we look at the half epoxy case, there is an extra wave envelope which is created before the original wave envelop. This extra wave signal in the unhealthy model is generated due to free space between steel and concrete, from where waves are reflected after reaching the boundary. The same behaviour was also observed by Akbas (2014 and 2016) during his study on the wave propagation in edge cracked functionally graded beams under impact force. After comparing the response signal at 50 kHz, investigations were carried out with 75 kHz frequency input excitation. It is observed that some more peaks are formed in this case. This may happen due to increase in noise level inside the concrete or steel shaft (of the anchor) after increase in frequency.

The wave propagation phenomena at different stages of the anchor systems considered in the present study (with an input wave frequency of 50 kHz) are depicted in Figs. 17-19. Distinct four stages of wave propagation from anchor head to the concrete surface are identified as, (a) wave reaches at the concrete surface through steel rod (b) wave reaches at the anchor end, (c) waves are propagating in to the concrete medium, (d) waves reach at the PZT sensors (receiver end). The time of flight for first waves to reach the concrete surface and at the end of steel rod inside concrete are same in all three cases as 40 μs (Figs. 17(a)-19(a) and

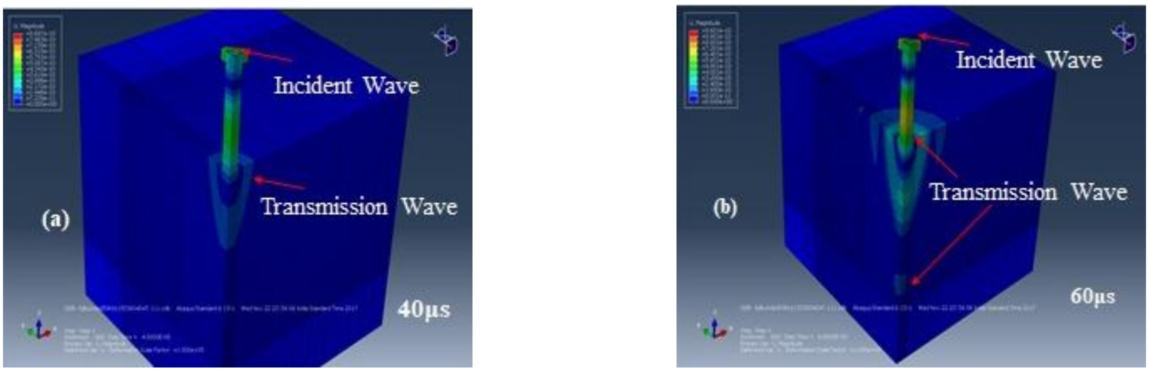

(a) Reaches the concrete surface (b) End of steel rod and started to reflect

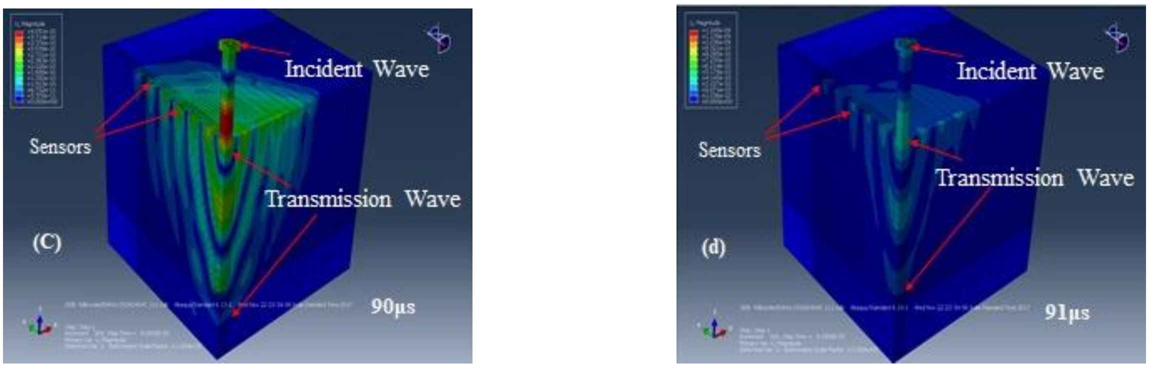

(c) and (d) Transmission of wave reaches at the sensors

Fig. 17 Wave propagation in full bonded model

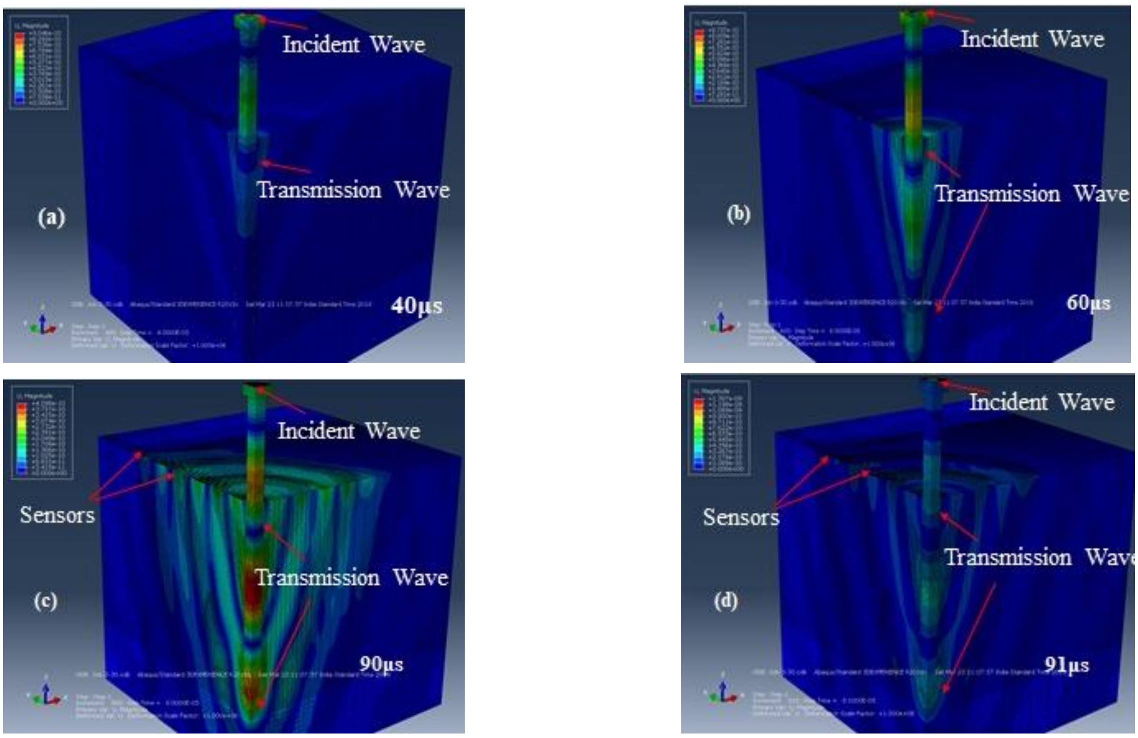

Fig. 18 Wave propagation in full epoxy model (a) reaches the concrete surface; (b) end of steel rod and started to reflect; (c) and (d) transmission of wave reaches at the sensors

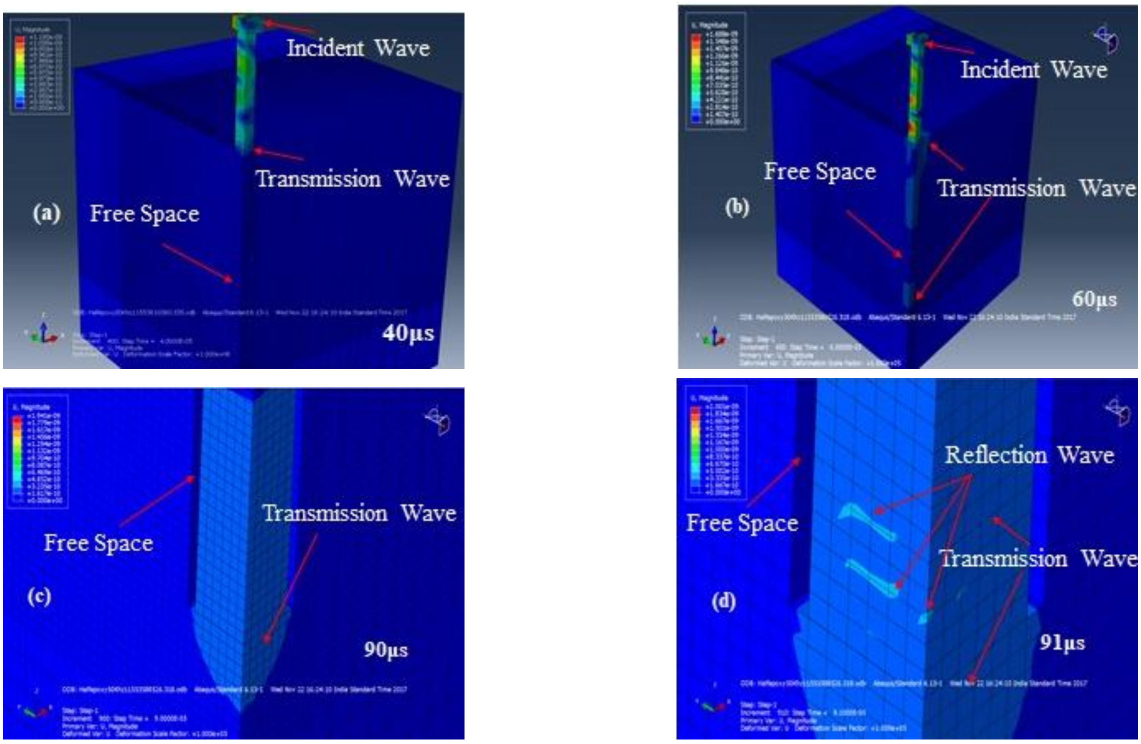

Fig. 19 Wave propagation in half epoxy (a) reaches the concrete surface; (b) end of steel rod and started to reflect; (c) wave transmission at 90 μs; (d) reflection from free space at 91 μs

Table 4 Time of fight at maximum amplitude at 50 kHz frequency

Model	Maximum amplitude (mV)		TOF at maximum amplitude (μs)	
	Sensor1	Sensor2	Sensor1	Sensor2
Full bonded	0.8516	0.7085	0.8516	0.7085
Full epoxy	0.6955	0.5795	0.6955	0.5795
Half epoxy	0.4595	0.5059	0.4595	0.5059

60 μs (Figs. 17(b)-19(b)) respectively as shown in Figs. 17-19. For detailed study on the wave propagation in the concrete-steel medium the state of wave at 90 μs (Figs. 17(c)-19(c)) and 91 μs (Figs. 17(d)-19(d)) are considered where the receiver sensors started to capture the response signals. It was observed that in full bonded and full epoxy case only transmission waves are propagating at 90 μs and 91 μs time of flight, while in half epoxy cases, reflection of waves was observed at 91 μs. This reflection of waves generating an extra wave packet is due to presence of crack inside the structure. The attenuation of waves can also be observed clearly from Figs. 17-19 in damage case. The time of flight (at 50 kHz) is also different for both sensors to attain the maximum peak values which are listed in Table 4. At both frequencies, the time of flight to attain the maximum peak in half epoxy model is much higher than other two models. However, if we look with respect to the intensity of wave propagation in full bonded (no epoxy) and full epoxy cases (both representing intact cases) are quite similar, but in case of half epoxy, most of energy seems to dissipate into the free space. Thus, the above study can provide a first hand and quick information on the presence of any invisible flaws inside embedment or integrity problem in the inaccessible anchor systems. To quantitatively assess the integrity of the chemical anchor system, the wave signals obtained from the study are further processed.

5.1 Analysis of results

There are many methods for the analysis of wave signals which can be judiciously employed for identifying the flaw/detect in the system. Most of them are used for straightforward and well-defined systems like metallic plate-like structures which may not hold good for complex and composite structures/systems. In this study, three methods are employed to assess the integrity of the concrete embedded anchor system based on the extent of requirement, the importance of the system and availability of tools.

5.1.1 Based on waveforms

The general method in which the waveforms are quantitatively compared is very simple and easiest way to compare one response with the other. In this method, all the response signals are plotted together as in Figs. 20-21. An extra wave envelope is identified in the half epoxy model before the formation of original wave envelops. The reason behind this is when waves are propagating along steel rod, part of waves reflects from the border of the steel and adhesive, while in other parts, the wave can propagate till the boundary without reflection (as depicted in Figs. 17-19). At the same time, multiple reflections from boundaries can be observed. After reflection from the boundaries, both

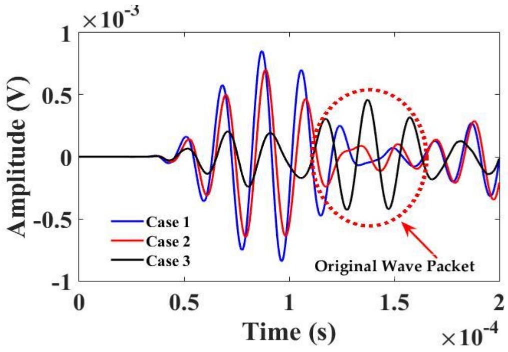

(a)

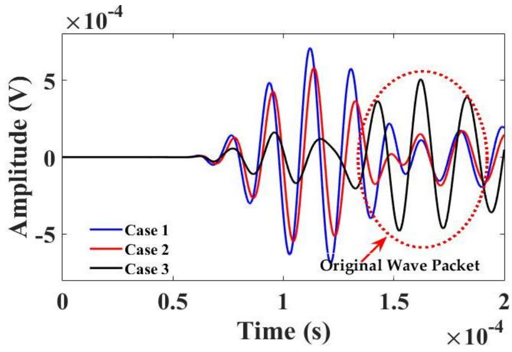

(b)

Fig. 20 Comparison between response signal for different model obtained at (a) S1; and (b) S2 at frequency 50 kH

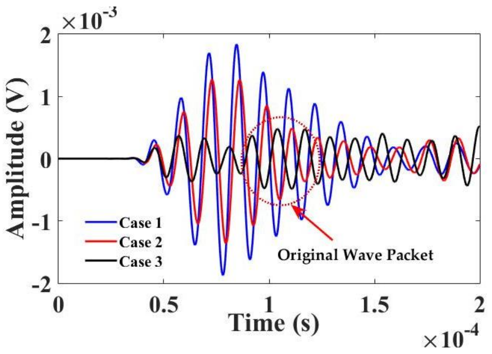

(a)

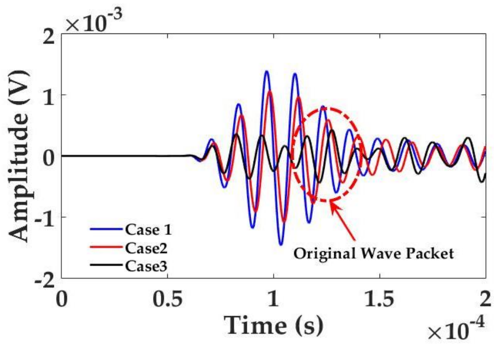

(b)

Fig. 21 Comparison between response signal for different model obtained at (a) S1; and (b) S2 at frequency 75k Hz

propagating and reflecting waves bounce back along the steel and concrete surface which causes the increase in the amplitude of waves. Therefore, some extra waves (forms and amplitude) are observed in half epoxy case.

5.1.2 Time Reversal Method (*TRM*)

Based on the above analysis, it is understood that the direct comparison between the output signal may lead to incorrect conclusion due to the influence of many parameters while capturing the signal. Therefore, it is important to highlight the genuine signal difference caused by damage for which Time Reversal method can be applied. The concept of time reversal was first introduced by the modern acoustic community for damage detection and potentially applied to many fields such as lithotripsy, ultrasonic brain surgery, underwater acoustic imaging and non-destructive testing (Gangadharan *et al*. 2009). Recently, attention has been paid towards time reversal method (TRM) in the field of guided wave-based techniques to improve the detectability of local defects in different composite structures (Agrahari and Kapuria 2016, Wang *et al*. 2015). Several research works are carried out theoretically as well as experimentally on different structures. Due to automatic compensation of loss of energy in damage and adaptability of time reversal, it can be used in any geometrical type of sensor. It is based on the wave propagation theory of time invariance and spatial linear reciprocity in any medium (Wang *et al*. 2010). The time reversal method for concrete embedded chemical anchor is

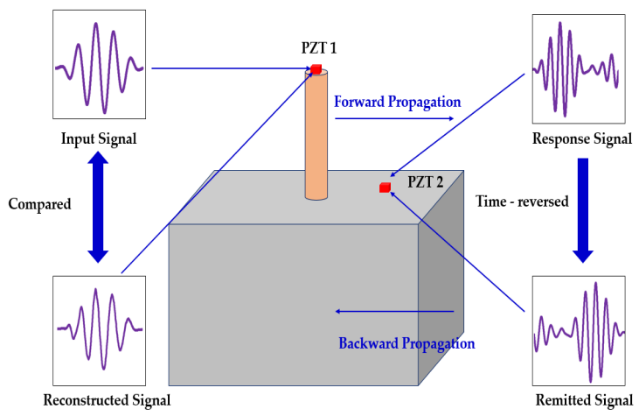

Fig. 22 Illustration of the time-reversal process

illustrated in Fig. 22, where an input signal is excited at PZT1 and the response signal is recorded at PZT 2. Now, this response signal is re-emitted after being reversed and scaled in a time domain as an excited signal at PZT 2. The compared with the original input excitation signal. If there is no damage present along the wave propagation path, the reconstructed signal should be almost similar as original excitation signal. It is important to note that, unlike a metallic plate problem, the signals cannot be identical here due to dispersion of wave propagation and mode conversions. However, it is interesting that, still the distortion in signal from damaged specimen can be clearly

Table 5 Normalised damage index range for a five-level scale (Kunnath *et al*. 1997)

Damage level	No damage	Light damage	Moderate damage	Strong damage	Collapse
Range for DI	0…0.1	0.1…0.24	0.25…0.4	0.4…1	≥ 1

identified. If any damage is present along the wave propagation path, not only the magnitude of wave propagation gets affected but also pattern of wave will change. The change in pattern and magnitude of wave leads to decrease in the similarity to the original signal.

Thus, it is important to calculate the damage index (DI) in the time reversal method. It is accomplished by comparing the waveform at different states, damaged and undamaged states, which shows the characteristic of wave signals in the time domain. The range of damage index for any structure varies between 0 (undamaged) to 1 (damaged). In the time domain, the change between two signals such as original excitation wave signal A = $\{a_1, a_2 \ldots\ldots a_n\}$ and reconstructed wave signal after time reversal B = $\{b_1, b_2 \ldots\ldots b_n\}$ can be quantitatively measured by correlation coefficients, is defined as (Wang *et al*. 2010)

$$\rho_{a,b}(t) = \frac{n\sum a_i\ b_i - \sum a_i \sum b_i}{\sqrt{\left[n\sum {a_i}^2 - (\sum a_i)^2\right]\left[n\sum {b_i}^2 - (\sum b_i)^2\right]}} \tag{12}$$

Where, $\rho_{a,b}(t)$ is defined by the degree of similarity between two signal A and B and n is the number of sample point in the time domain. Before the analysis, reconstructed signals are normalised to compensate for the dispersion of wave energy. $\rho_{a,b}(t) = 1$ shows that each signal is perfectly approximated by the other. The damage index can be calculated by subtracting the degree of similarity from unity.

$$\mathrm{DI} = 1 - \rho_{a,b}(t) \tag{13}$$

Higher values of DI indicates the greater possibility of existence damage. The damage index has been categorized by Kunnath *et al*. (1997) for five-level scale shown in below Table 5. Results are shown in Figs. 23 and 24 at two frequencies 50 kHz and 75 kHz for detecting the presence of damage inside the structures. It is significant to mention that the figures depict a distinctly different and extremely distorted wave signature obtained from the third anchor system (half-epoxy) and it independently indicates the presence of damage or flaw in the third anchor system.

The similarity and the damage indices among the different anchor cases at 50 kHz and 75 kHz are presented in Table 6. It is found that maximum similarity (DI = 0) can be achieved in case of full bonded and full epoxy model at both excitation frequencies and the third case (half- epoxy)

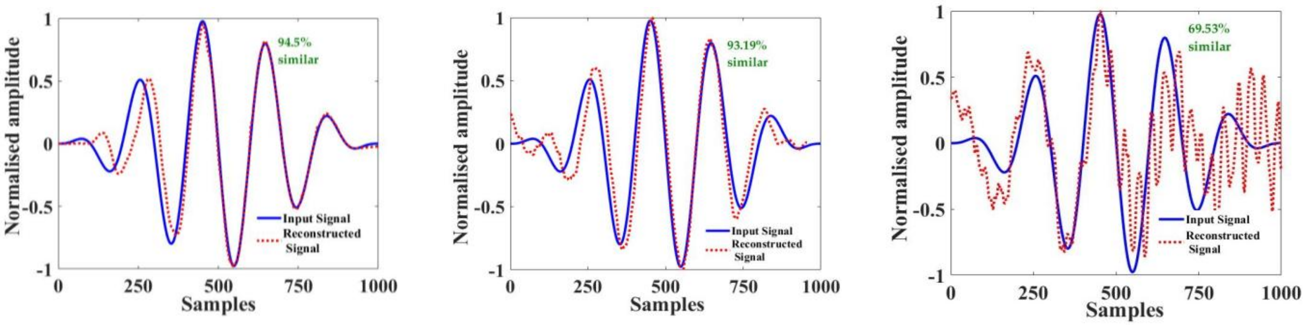

(a) (b) (c)

Fig. 23 Comparison of the input signal and reconstructed signal (a) full bonded model; (b) full epoxy model; (c) half epoxy or damage model at frequency 50 kHz

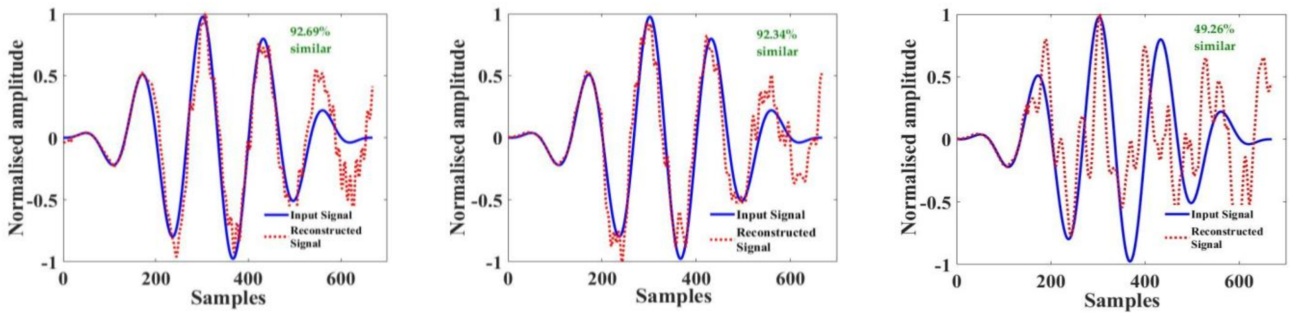

(a) (b) (c)

Fig. 24 Comparison of the input signal and reconstructed signal (a) full bonded model; (b) full epoxy model; (c) half epoxy or damage model at frequency 75 kHz and distinctly identifies the clear damage in the half epoxy shows very low similarity. Further, the damage index points out the near zero damage in first two cases, and successfully case. With respect to damage index, we can compare with normalized damage index for a five-level scale given by Kunnath *et al*. (1997) and have observed that at both frequencies ranges half epoxy model shows the moderate to severe damage.

5.1.3 Temporal residual energy using signal reversal Method

Time domain differentiation method can be employed for quantitatively comparing two propagating wave signals within fixed time length. This is a simple but promising method to compare the two signals. However, to obtain the most accurate result, these differencing signals must be independent of the original signals (normalised) as well as these signals should be approximately scaled (Michaels and Michaels 2005). Satisfying the above conditions, the measured signal is scaled to unit energy, while reference signal is scaled to minimizing the error between two signals. A scale factor (α) is calculated for reference signal to enhance the energy up to measured signals. In this method, two ultrasonic signals, $x(t)$ and $y(t)$, both of length T, is considered. Where $x(t)$ is the measured signal and $y(t)$ is the baseline signal. The sample signals are $x(n)$ and $y(n)$, where n corresponds to the sample at time n/f_s, and the length is $N = f_s T$, and f_s is the sampling frequency. Time domain differencing is calculated as

$$d(n) = x(n) - y(n) \tag{14}$$

Where $d(n)$ is the difference in signals and scaled signals can be calculated as below

Table 6 Similarity and damage index for a different model at 50 and 75 kHz frequency

Model	Similarity (in %)		Damage Index	
	50 kHz	75 kHz	50 kHz	75 kHz
Full bonded model	94.50	92.69	0.0550	0.0731
Full epoxy model	93.19	92.34	0.0681	0.0766
Half epoxy	69.53	49.26	**0.3047**	**0.5074**

$$\tilde{x}(n) = \frac{x(n)}{\sqrt{\sum_{N=1}^{N=n} x^2(n)}} \tag{15}$$

$$\alpha = \frac{\sum_{N=1}^{N=n} \tilde{x}(n) y(n)}{\sum_{N=1}^{N=n} y^2(n)} \tag{16}$$

$$\tilde{d}(n) = \tilde{x}(n) - \alpha . y(n) \tag{17}$$

Where, $\tilde{x}(n)$ is the unity energy measured signal, α is scale factor for reference signal or baseline signal and $\tilde{d}(n)$ is an amplitude independent signal. The energy left out within a specified time window also termed as temporal residual energy is calculated as

$$E = \sum_{N=1}^{N=n} \tilde{d}^2(n) \tag{18}$$

To calculate the temporal residual energy, the first signal which is obtained by sensor 1 (output1) on the concrete surface is considered as a reference signal when excitation is given by actuator at the top surface of steel rod head as shown in Fig. 25(a). Another signal which is obtained at the top surface (head) of the anchor (output2) while excitation signal is given through actuator at the concrete surface is considered as a measured signal as shown in Fig. 25(b). In both conditions, given excitation signals are same.

Temporal residual energy method is used to compare the signals by making the signal energy to unity. It has been clearly observed from the Figs. 26-27 that the difference of scaled signal for full bonded and full epoxy case approximately tends to zero. It signifies that after scaling the signal to unity, the amplitude of measured and reference signal is almost same. While in half epoxy case, there is a significant difference between the measured and reference signal after scaling, which indicates that there is loss of energy during its transmission through the half-bonded epoxy section. From Table 7, it can be observed that the most dissipation of energy is in half epoxy case as the scale factor (α) is highest while least dissipation of energy is found to be from full bonded case. This means, the attenuation of wave energy is highest in case of half epoxy model while least in case of the full bonded model. The

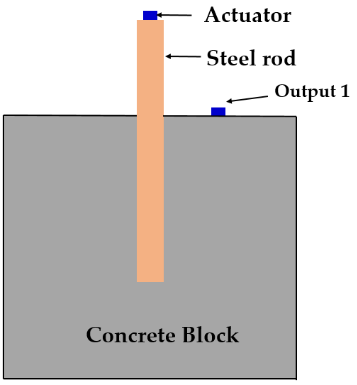

(a)

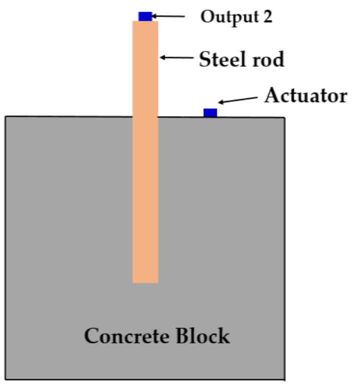

(b)

Fig. 25 Full bonded 2-D model when (a) actuator is at the top surface of steel rod; and (b) actuator is at the concrete surface

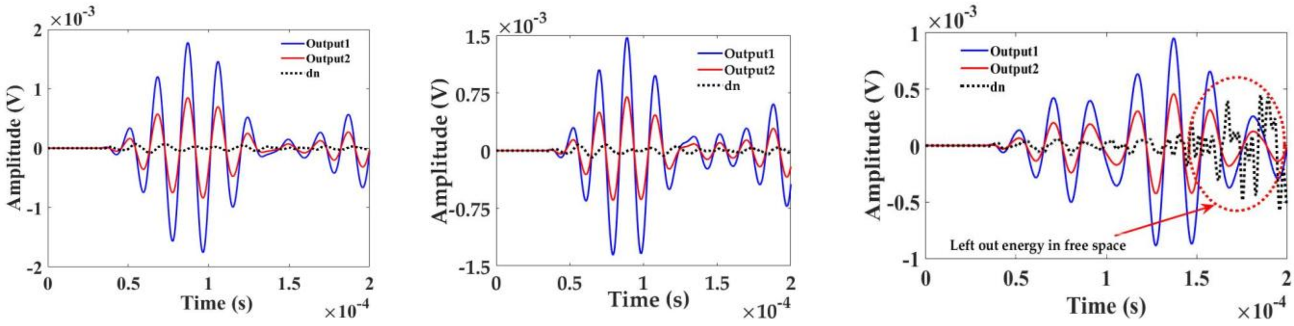

(a) (b) (c)

Fig. 26 Time differencing of two output for (a) full bonded model; (b) full epoxy model; and (c) half epoxy or damage model at a 50 kHz sampling frequency (dn is residual energy)

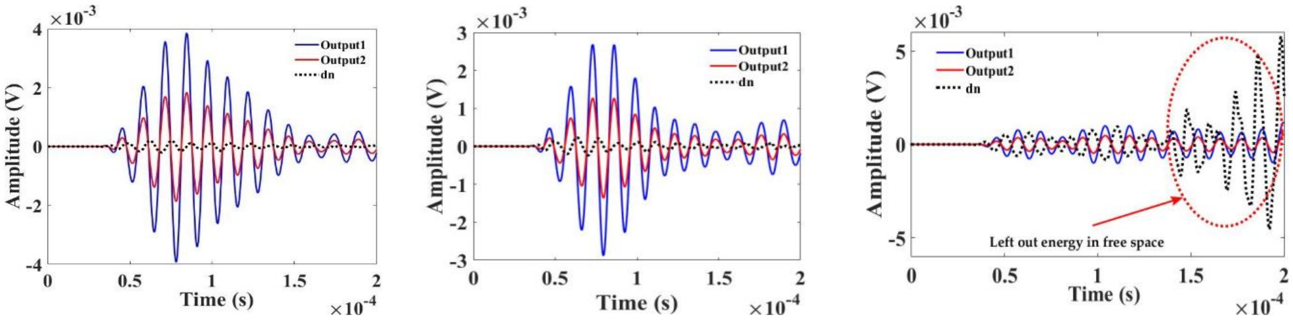

(a) (b) (c)

Fig. 27 Time differencing of two output for (a) full bonded model; (b) full epoxy model; and (c) half epoxy or damage model at a 75 kHz sampling frequency (dn is residual energy)

Table 7 Scale factor (α) for refernce signal and temporal residual energy (E)

Model	Scale factor (α)		Temporal residual energy (E)	
	50 kHz	75 kHz	50 kHz	75 kHz
Full bonded	77.93995262	36.13929181	1.34815E-06	9.23402E-06
Full epoxy	96.3490209	53.78402343	1.784E-06	1.08497E-05
Half epoxy	137.0625022	97.57547151	**3.11E-05**	**0.003036856**

temporal residual energy which is also known as left out energy inside the structures is higher in a system with a flaw. It is interesting to note that, out of the two input excitation frequencies, the difference in residual energy in damage model is significantly higher than other two systems which can be distinctly observed without any reference.

6. Conclusions

In the present study, elaborate computational investigations are carried out to establish the feasibility of assessing the integrity of chemical anchor system (embedded in concrete with adhesive interface) by using simulated guided wave propagation technique. Numerical studies are carried out on three different anchor models at different frequency levels (12.5-100 kHz) and constant excitation signal (20V) using piezoelectric transducers. The study is focused to recognize the phenomenon of the wave energy transferred between steel-adhesive-concrete interfaces. The following are the major observations made and conclusions drawn from the present study:

Experimentally validated numerical models are used to develop an appropriate methodology for damage (flaw) detection in chemical anchors embedded in concrete where the anchor head and the surrounding concrete are only accessible. The results obtained from the numerical studies are reasonably well matched with the experimental results.

- To detect the damage present in the interior (embedded) part of the chemical anchor using ultrasonic wave propagation, different methods and detection algorithms can be effectively employed for getting the damage information from the wave characteristics.
- Experimentally it is found that, due to the presence of different materials and highly attenuating nature of concrete and composite layers, the low-frequency signal is not able to obtain any distinct response; while due to scattering at high frequency, it is difficult to differentiate among the reflecting and propagating waves. However, the frequency range

50-75 kHz is found to be suitable and can be used for damage detection in chemical anchors embedded in concrete.
- Numerical studies brings out that the fast hand information can be obtained from the significant deviation in the original wave packet (from received signals) in case of damage system.
- Further, the Time Reversal Method shows the great potential to be employed for damage detection in such complex systems, where damage index could be able to reflect the extent of damage.
- Using the temporal residual energy, it is found that the scale factor (α) is very high for the half epoxy case in comparison of other cases which indicates the transmission of energies between interfaces is very less due to debonding.
- It is significant to note that no baseline information is required to identify the damaged (with flaw) system and presence of damage can be easily detectable by properly investigating the received signal characteristics.
- It is also to be mentioned that though a quarter model is used in the present study, the entire study is extremely computationally intensive due to the nature of analysis (wave propagation), large number of elements and interfaces of materials of two different properties.
- The study brings out that by using proper numerical models and wave propagation parameters, it is possible to assess the integrity of the chemical anchors which has huge practical usages.
- It is important to mention that some assumptions are made in the numerical investigations carried out in the present study (as mentioned in the preceeding sections), such as (i) flaw is concentrated and not spread (distributed), (ii) dimensions and the properties of all components (anchor, adhesive and concrete) are known, (iii) surrounding concrete is homogeneous and effect due to presence of coarse aggregate is not considered, (iv) flaw is developed only due to adhesive. The promising observations of the present study would encourage to take up further and more generalised studies which may systematically address the above mentioned limitations of the present work.

Acknowledgments

The authors would like to acknowledge the help received from Ms. A. Thirumalaiselvi, Scientist for analytical studies and the stuff of Special and Multifunctional Structures Laboratory, CSIR-SERC during casting of specimens and conducting experiments.

References

Adams, D. (2007), *Health monitoring of structural materials and components: methods with applications*, John Wiley & Sons.

Agrahari, J.K. and Kapuria, S. (2016), "A refined Lamb wave time-reversal method with enhanced sensitivity for damage detection in isotropic plates", *J. Intel. Mater. Syst. Struct.*, **27**(10), 1283-1305.

Akbaş, Ş.D. (2014), "Wave propagation analysis of edge cracked circular beams under impact force", *PloS one*, **9**(6), e100496.

Akbas, S.D. (2015), "Wave propagation of a functionally graded beam in thermal environments", *Steel Compos. Struct., Int. J.*, **19**(6), 1421-1447.

Akbaş, Ş.D. (2016), "Wave propagation in edge cracked functionally graded beams under impact force", *J. Vib. Control*, **22**(10), 2443-2457.

Amjad, U., Yadav, S.K. and Kundu, T. (2015), "Detection and quantification of diameter reduction due to corrosion in reinforcing steel bars", *Struct. Health Monitor.*, **14**(5), 532-543.

Chalioris, C.E., Papadopoulos, N.A., Angeli, G.M., Karayannis, C.G., Liolios, A.A. and Providakis, C.P. (2015), "Damage evaluation in shear-critical reinforced concrete beam using piezoelectric transducers as smart aggregates", *Open Eng.*, **5**(1), 373-384

Contrafatto, L. and Cosenza, R. (2014), "Behaviour of post-installed adhesive anchors in natural stone", *Constr. Build. Mater.*, **68**, 355-369.

Cook, R.A. (1993), "Behavior of chemically bonded anchors", *J. Struct. Eng.*, **119**(9), 2744-2762.

Cui, Y. and Zou, D.H. (2015), "Assessing the effect of insufficient rebar and missing grout in grouted rock bolts using guided ultrasonic waves", *J. Appl. Geophys.*, **79**, 64-70.

Epackachi, S., Esmaili, O., Mirghaderi, S.R. and Behbahani, A.A.T. (2015), "Behavior of adhesive bonded anchors under tension and shear loads", *J. Constr. Steel Res.*, **114**, 269-280.

Fourn, H., Atmane, H.A., Bourada, M., Bousahla, A.A., Tounsi, A. and Mahmoud, S.R. (2018), "A novel four variable refined plate theory for wave propagation in functionally graded material plates", *Steel Compos. Struct., Int. J.*, **27**(1), 109-122.

Gangadharan, R., Murthy, C.R.L., Gopalakrishnan, S. and Bhat, M.R. (2009), "Time reversal technique for health monitoring of metallic structure using Lamb waves", *Ultrasonic*, **49**(8), 696-705.

Giurgiutiu, V. (2011), "Structural damage detection with piezoelectric wafer active sensors", In: *Journal of Physics: Conference Series*, Vol. 305, No. 1, p. 012123.

Gou, H.Y., Wang, W., Shi, X.Y., Pu, Q.H. and Kang, R. (2018), "Behavior of steel-concrete composite cable anchorage system", *Steel Compos. Struct., Int. J.*, **26**(1), 115-123.

Gu, A., Luo, Y. and Xu, B. (2016), "Continuous condition monitoring of reinforced concrete using an active diagnosis method", *Struct. Health Monitor.*, **15**(1), 104-112.

Hall, J. and Michaels, J. (2015), "Multipath ultrasonic guided wave imaging in complex structures", *Struct. Health Monitor.*, **14**(4), 345-358.

Han, S., Palazotto, A.N. and Leakeas, C.L. (2009), "Finite-element analysis of Lamb wave propagation in a thin aluminum plate", *J. Aerosp. Eng.*, **22**(2), 185-197.

Haynes, C., Todd, M., Nadabe, T. and Takeda, N. (2014), "Monitoring of bearing failure in composite bolted connections using ultrasonic guided waves: A parametric study", *Struct. Health Monitor.*, **13**(1), 94-105.

Hsiao, C., Cheng, C.C., Liou, T. and Juang, Y. (2008), "Detecting flaws in concrete blocks using the impact-echo method", *NDT & E International*, **41**(2), 98-107.

Ihn, J.B. and Chang, F.K. (2008), "Pitch-catch active sensing methods in structural health monitoring for aircraft structures", *Struct. Health Monitor.*, **7**(1), 5-19

Karayannis, C.G., Chalioris, C.E., Angeli, G.M., Papadopoulos, N.A., Favvata, M.J. and Providakis, C.P. (2016), "Experimental damage evaluation of reinforced concrete steel bars using piezoelectric sensors", *Constr. Build. Mater.*, **105**, 227-244

Kocaturk, T. and Akbas, S.D. (2013), “Wave propagation in a microbeam based on the modified couple stress theory”, *Struct. Eng. Mech., Int. J.*, **46**(3), 417-431.

Kunnath, S.K., El-Bahy, A., Taylor, A. and Stone, W. (1997), *Cumulative seismic damage of reinforced concrete bridge piers*.

Lee, F.W., Chai, H.K. and Lim, K.S. (2017), “Characterizing concrete surface notch using Rayleigh wave phase velocity and wavelet parametric analyses”, *Constr. Build. Mater.*, **136**, 627-642.

Li, J., Lu, Y., Guan, R. and Qu, W. (2017), “Guided waves for debonding identification in CFRP-reinforced concrete beams”, *Constr. Build. Mater.*, **131**, 388-399.

Liu, Z., Sun, K., Song, G., He, C. and Wu, B. (2016), “Damage localization in aluminum plate with compact rectangular phased piezoelectric transducer array”, *Mech. Syst. Signal Process.*, **70-71**, 625-636.

Michaels, J.E. and Michaels, T.E. (2005), “Detection of structural damage from the local temporal coherence of diffuse ultrasonic signals”, *IEEE Transactions on Ultrasonic, Ferroelectrics, and Frequency Control*, **52**(10), 1769-1782.

Mohseni, H. and Ng, C.T. (2018), “Rayleigh wave propagation and scattering characteristics at debonding in fibre-reinforced polymer-retrofitted concrete structures”, *Struct. Health Monitor.*, 1475921718754371.

Mustapha, S., Lu, Y., Li, J. and Ye, L. (2014), “Damage detection in rebar-reinforced concrete beams based on time reversal of guided waves”, *Struct. Health Monitor.*, **13**(4), 347-358

Neilson, R.D., Ivanović, A., Starkey, A.J. and Rodger, A.A. (2007), “Design and dynamic analysis of a pneumatic impulse generating device for the non-destructive testing of ground anchorages”, *Mech. Syst. Signal Process.*, **21**(6), 2523-2545.

Paknahad, M., Shariati, M., Sedghi, Y., Bazzaz, M. and Khorami, M. (2018), “Shear capacity equation for channel shear connectors in steel-concrete composite beams”, *Steel Compos. Struct., Int. J.*, **28**(4), 483-494.

Papastergiou, D. and Lebet, J.-P. (2014), “Investigation of a new steel-concrete connection for composite bridges”, *Steel Compos. Struct., Int. J.*, **17**(5), 573-599.

Park, H.W., Sohn, H., Law, K.H. and Farrar, C.R. (2007), “Time reversal active sensing for health monitoring of a composite plate”, *J. Sound Vib.*, **302**(1-2), 50-66.

Prior, A.M. (1994), “Application of implicit and explicit finite element techniques to metal forming”, *J. Mater. Process. Technol.*, **45**, 649-656

Providakis, C.P., Angeli, G.M., Favvata, M.J., Papadopoulos, N.A., Chalioris, C.E. and Karayannis, C.G. (2014), “Detection of concrete reinforcement damage using piezoelectric materials-Analytical and experimental study”, *Int. J. Civil Architect. Struct. Constr. Eng.*, **8**(2), 197-205.

Puigvert, F., Crocombe, A.D. and Gil, L. (2014), “Static analysis of adhesively bonded anchorages for CFRP tendons”, *Constr. Build. Mater.*, **61**, 206-215.

Raghavan, A. (2007), “Review of guided-wave structural health monitoring”, *Shock Vib. Digest*, **39**(2), 91-114.

Rajeshwara, C.S., Banerjee, S. and Lu, Y. (2017), “Identification of Zero Effect State in Corroded RCC Structures Using Guided Waves and Embedded Piezoelectric Wafer Transducers (PWT)”, *Procedia Eng.*, **188**, 209-216.

Rizzo, P., Spada, A., Degala, S. and Giambanco, G. (2010), “Acoustic emission monitoring of chemically bonded anchors”, *J. Non-Destruct. Eval.*, **29**(1), 49-61.

Rong, X., Lin, P., Liu, J. and Yang, T. (2017), “A New Approach of Waveform Interpretation Applied in Non-destructive Testing of Defects in Rock Bolts Based on Mode Identification”, *Math. Problems Eng.*

Rose, J.L. (2004), *Ultrasonic Waves in Solid Media*, Cambridge University Press.

Rucka, M. and Zima, B. (2015), “Elastic wave propagation for condition assessment of steel bar embedded in mortar”, *Int. J. Appl. Mech. Eng.*, **20**(1), 159-170.

Sasmal, S., Thiyagarajan, R., Lieberum, K.H. and Koenders, E.A.B. (2018), “Numerical simulations of progression of damage in concrete embedded chemical anchors”, *Comput. Concrete, Int. J.*, **22**(4), 395-405.

Divsholi, B.S. and Yang, Y. (2008), “Application of PZT Sensors for Detection of Damage Severity and Location in Concrete”, *Proceedings of the SPIE, The International Society for Optical Engineering*, Vol. 7268, Art. No. 726813

Seifried, R., Jacobs, L.J. and Qu, J. (2002), “Propagation of guided waves in adhesive bonded components”, *NDT & E International*, **35**(5), 317-328.

Shen, W., Li, D. and Ou, J. (2018), “Numerical simulation of guided wave propagation in reinforced concrete structures with debond damage”, In: *Non-destructive Characterization and Monitoring of Advanced Materials, Aerospace, Civil Infrastructure, and Transportation XII*, Vol. 10599, 105991H; International Society for Optics and Photonics.

Song, G., Mo, Y.L., Otero, K. and Gu, H. (2006), “Health monitoring and rehabilitation of a concrete structure using intelligent materials”, *Smart Mater. Struct.*, **15**(2), 309.

Song, G., Gu, H., Mo, Y.L., Hsu, T.T.C. and Dhonde, H. (2007), “Concrete structural health monitoring using embedded piezoceramic transucers”, *Smart Mater. Struct.*, **16**(4), 959.

Song, F., Huang, G.L., Kim, J.H. and Haran, S. (2008a), “On the study of surface wave propagation in concrete structures using a piezoelectric actuator/sensor system”, *Smart Mater. Struct.*, **17**(5), 055024.

Song, G., Gu, H. and Mo, Y.L. (2008b), “Smart aggregates: Multi-functional sensors for concrete structures-a tutorial and a review”, *Smart Mater. Struct.*, **17**, 1-17.

Song, G., Li, W., Wang, B. and Ho, S.C.M. (2017), “A review of rock bolt monitoring using smart sensors”, *Sensors*, **17**(4), 776.

Staszewski, W.J., Lee, B.C., Mallet, L. and Scarpa, F. (2004), “Structural health monitoring using scanning laser vibrometry: I. Lamb wave sensing”, *Smart Mater. Struct.*, **13**(2), 251.

Tawie, R. and Lee, H.K. (2010), “Piezoelectric-Based Non-Destructive Monitoring of Hydration of Reinforced Concrete as an Indicator of Bond Development at the Steel–Concrete Interface”, *Cement Concrete Res.*, **40**(12), 1697-1703.

Thirumalaiselvi, A., Anandavalli, N., Rajasankar, J. and Iyer, N.R. (2016), “Numerical evaluation of deformation capacity of laced steel concrete composite beams under monotonic loading”, *Steel Compos. Struct., Int. J.*, **20**(1), 167-184

Wang, C., He, W., Ning, J. and Zhang, C. (2009), “Propagation properties of guided wave in the anchorage structure of rock bolts”, *J. Appl. Geophys.*, **69**(3-4), 131-139.

Wang, D., Ye, L., Su, Z., Lu, Y., Li, F. and Meng, G. (2010), “Probabilistic damage identification based on correlation analysis using guided wave signals in aluminum plates”, *Struct. Health Monitor.*, **9**(2), 133-144.

Wang, R.L., Gu, H., Mo, Y.L. and Song, G. (2013), “Proof-of-concept experimental study of damage detection of concrete piles using embedded piezoceramic transducers”, *Smart Mater. Struct.*, **22**(4), 042001.

Wang, Q., Yuan, S., Hong, M. and Su, Z. (2015), “On time reversal-based signal enhancement for active lamb wave-based damage identification”, *Smart Struct. Syst., Int. J.*, **15**(6), 1463-1479.

Wu, F. and Chang, F.K. (2006), “Debond detection using embedded piezoelectric elements in reinforced concrete structures-part I: experiment”, *Struct. Health Monitor.*, **5**(1), 5-15.

Xu, B., Chen, H., Mo, Y.L. and Chen, X. (2017), “Multi-physical field guided wave simulation for circular concrete-filled steel tubes coupled with piezoelectric patches considering debonding defects", *Int. J. Solids Struct.*, **122**, 25-32.

Yan, S., Sun, W., Song, G.B., Gu, H.C., Huo, L.S., Liu, B. and Zhang, Y.G. (2009), "Health monitoring of reinforced concrete shear walls using smart aggregates", *Smart Mater. Struct.*, **18**, 1-6.

Yang, Y., Hu, Y. and Lu, Y. (2008), "Sensitivity of PZT Impedance Sensors for Damage Detection of Concrete Structures", *Sensors*, **8**, 327-346.

Yilmaz, S., Ö zen, M.A. and Yardim, Y. (2013), "Tensile behavior of post-installed chemical anchors embedded to low strength concrete", *Constr. Build. Mater.*, **47**, 861-866.

Yu, J.D., Bae, M.H., Lee, I.M. and Lee, J.S. (2013), "Nongrouted ratio evaluation of rock bolts by reflection of guided ultrasonic waves", *J. Geotech. Geoenviron. Eng.*, **139**, 298-307.

Zhang, J., Xu, J., Guan, W. and Du, G. (2018), "Damage Detection of Concrete-Filled Square Steel Tube (CFSST) Column Joints under Cyclic Loading Using Piezoceramic Transducers", *Sensors*, **18**(10), 3266.

Zheng, Z. and Lei, Y. (2014), "Effects of concrete on propagation characteristics of guided wave in steel bar embedded in concrete", *Shock Vib.*

Zima, B. and Rucka, M. (2015), "Wave propagation in damage assessment of ground anchors", In: *Journal of Physics: Conference Series*, **628**(1), 012026; IOP Publishing.

Zou, D.S., Cheng, J., Yue, R. and Sun, X. (2010), "Grout quality and its impact on guided ultrasonic waves in grouted rock bolts", *J. Appl. Geophys.*, **72**(2), 102-106.

CC